Journal of
**Applied Crystallography**
ISSN 0021-8898

Received 16 August 2006
Accepted 8 November 2006

# Synchrotron X-ray reflectivity studies of nanoporous organosilicate thin films with low dielectric constants

**Weontae Oh,[a] Yongtaek Hwang,[b] Tae Joo Shin,[b] Byeongdu Lee,[b] Jong-Seong Kim,[b] Jinhwan Yoon,[b] Sean Brennan,[c] Apurva Mehta[c] and Moonhor Ree[b]***

[a]Department of NanoTechnology, Dong-eui University, Busan 614-714, Republic of Korea, [b]Department of Chemistry, National Research Lab for Polymer Synthesis and Physics, Pohang Accelerator Laboratory, Center for Integrated Molecular Systems, and BK School of Molecular Science, Pohang University of Science and Technology (Postech), Pohang 790-784, Republic of Korea, and [c]Stanford Synchrotron Radiation Laboratory, MS 69, PO Box 20450, Stanford, CA 94209, USA. Correspondence e-mail: ree@postech.edu

Quantitative, non-destructive X-ray reflectivity analysis using synchrotron radiation sources was successfully performed on nanoporous dielectric thin films prepared by thermal processing of blend films of a thermally curable polymethylsilsesquioxane dielectric precursor and a thermally labile triethoxysilyl-terminated six-arm poly($\varepsilon$-caprolactone) porogen in various compositions. In addition, thermogravimetric analysis and transmission electron microscopy analysis were carried out. These measurements provided important structural information about the nanoporous films. The thermal process used in this study was found to cause the porogen molecules to undergo efficiently sacrificial thermal degradation, generating closed, spherical nanopores in the dielectric film. The resultant nanoporous films exhibited a homogeneous, well defined structure with a thin skin layer and low surface roughness. In particular, no skin layer was formed in the porous film imprinted using a porogen loading of 30 wt%. The film porosities ranged from 0 to 33.8% over the porogen loading range of 0–30 wt%.



## 1. Introduction

Porous organosilicate thin films have recently attracted much interest due to their potential applications as low dielectric constant (low-$k$) interdielectric layers (Lee, Oh, Hwang *et al.*, 2005; Lee, Oh, Yoon *et al.*, 2005; Lee, Park *et al.*, 2005; Lee, Yoon *et al.*, 2005; Ree *et al.*, 2006), chemical and biosensor membranes (Rottman *et al.*, 1999; de Morais *et al.*, 1999), catalyst hosts (Harmer *et al.*, 1996; Lev *et al.*, 1995), and gas separation membranes (Smaihi *et al.*, 1996). A well-known method for preparing porous organosilicates is to first perform the templated sol-gel synthesis of organosilanes in the presence of labile porogens (*i.e.*, pore generators) such as organic surfactants and polymers, and then to remove the porogen templates so as to generate pores in the resultant organosilicates (Bolze *et al.*, 2001; Huang *et al.*, 2002; Lee *et al.*, 2002; Oh *et al.*, 2003). In particular, incorporating nanometer-sized, air-filled pores (so-called closed nanopores) of $k$ = 1.01 into an interdielectric thin film layer is a potential method for significantly reducing the $k$ value of the film (Bolze *et al.*, 2001; Huang *et al.*, 2002; Lee *et al.*, 2002; Oh *et al.*, 2003). Multi-armed poly($\varepsilon$-caprolactone)s (PCLs) have been widely investigated as thermally labile organic polymer porogen agents for organosilicate dielectrics such as polymethylsilsesquioxane (PMSSQ) (Bolze *et al.*, 2001; Oh *et al.*, 2003). These porogens undergo sacrificial thermal decomposition in the temperature range 523–623 K; however, the large number of arms in these compounds was found to result in severe aggregation, even at a loading of 10 wt%, leading to the formation of large interconnected pores in the dielectric thin films (Ree *et al.*, 2006). This tendency of multi-armed PCLs toward aggregation in organosilicates has limited the pore size and porosity that can be achieved using these compounds, and has obviated their use in advanced integrated circuits (ICs) patterned with small feature sizes. Thus, in order to develop advanced ICs, a method is required to generate dielectric materials containing a uniform distribution of closed pores with dimensions significantly smaller than the feature size. Moreover, the ability to characterize the structure of the porous film, in particular the pore structure and distribution within the film, is as important as developing the dielectrics and porogens themselves.

In the present study, we prepared porous organosilicate dielectric thin films from a triethoxysilyl-terminated six-armed PCL (mPCL6) and PMSSQ dielectric precursor (Fig. 1), and quantitatively investigated their structures, surface roughnesses, and electron density gradients along the film thickness using specular X-ray reflectivity (XR) with synchrotron radiation sources. In addition, we performed transmission electron microscopy (TEM) on the porous films, and thermogravimetric analysis (TGA) on some of the dried films. As seen in Fig. 1, the triethoxysilyl terminal groups on the mPCL6 porogen are analogues of the reactive functional groups (ethoxysilyl and hydroxysilyl) of the PMSSQ precursor that take part in the curing reaction (*i.e.* the secondary polycondensation reaction) during heat-treatment. Owing to the similarity of these reactive functional groups, the porogen is more miscible with the PMSSQ precursor and, furthermore, the triethoxysilyl terminal groups cause the porogen to participate in the curing reaction of the PMSSQ precursor, leading to a significant reduction in aggregation in these blend films. The

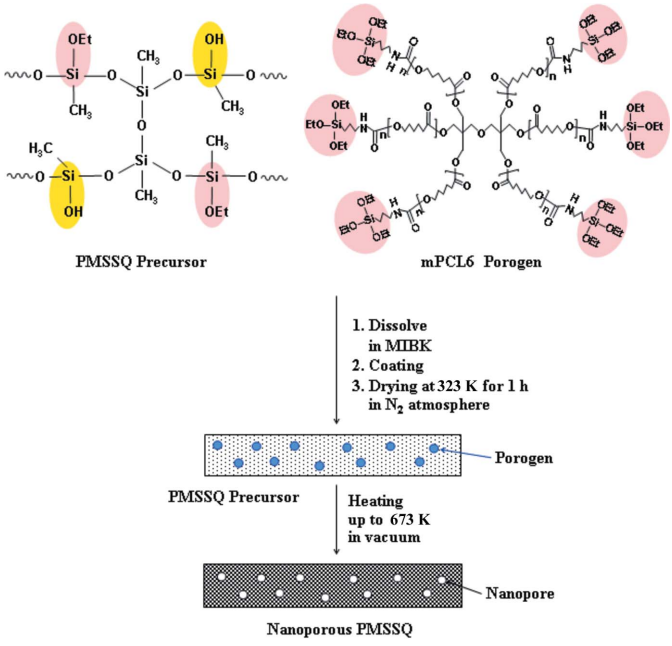


**Figure 1**
Procedure for the preparation on nanoporous dielectric thin films from the PMSSQ precursor (curable dielectric matrix) and triethoxysilyl-terminated star-shaped PCL porogen (mPCL6, thermally labile porogen).

resulting porogen aggregates are therefore smaller than has been achieved in the past. After sacrificial thermal degradation, the aggregates leave their footprints in the cured PMSSQ dielectric films as nanopores.

## 2. Experiment

A mPCL6 porogen [triethoxysilyl-terminated six-arm poly($\varepsilon$-caprolactone)] was synthesized and found to have a weight-average molecular weight $\overline{M_w}$ of 9600 and a polydispersity index of 1.11 (Lee, Oh & Hwang *et al.*, 2005; Lee, Oh & Yoon *et al.*, 2005; Shin *et al.*, 2001). A soluble PMSSQ dielectric precursor ($\overline{M_w}$ = 10000) containing ethoxysilyl and hydroxysilyl groups (GR650F) was supplied by Techneglas (Perrysburg, OH). A series of homogeneous solutions of mPCL6 porogen and PMSSQ precursor in dry methyl isobutyl ketone (MIBK) (5 wt% solid) was prepared using porogen compositions of 10, 20 and 30 wt%. Each solution was filtered with a PTFE-membrane microfilter of pore size 0.20 µm, spin-coated onto a precleaned silicon substrate, and then dried at 323 K for 1 h under a nitrogen atmosphere (Fig. 1). The dried thin films were heated to 473 K at a rate of 2.0 K $min^{-1}$ and thermally cured at that temperature for 100 min. Then, the films were further heated to 673 K at a rate of 2.0 K $min^{-1}$ and kept at 673 K for 1 h; during this heat treatment, the porogen component in the films underwent thermal decomposition, generating pores in the films. The whole thermal process was conducted in a vacuum (Fig. 1).

Specular XR measurements were conducted using synchrotron radiation sources at the bending magnet X-ray diffraction beamlines BL3C2 and BL4C2 of the Pohang Light Source in Korea (Bolze *et al.*, 2002; Hwang *et al.*, 2006; Lee *et al.*, 2004; Ree & Ko, 2005) and at the bending magnet X-ray diffraction beamline BL2-1 of the Stanford Radiation Research Laboratory in the USA. The X-ray radiation source was selected to be a wavelength $\lambda$ of 1.54 Å in an energy resolution of $\Delta\lambda/\lambda = 5 \times 10^{-4}$ and a scintillation counter with an enhanced dynamic range (Bede Scientific, EDR) was used as a detector. XR data were collected in a specular direction by a $\theta$–$2\theta$ scan and then normalized to the intensity of the incident X-ray beam monitored using an ionization chamber. Particular care was taken with the sample alignment to ensure precision, as described by Gibaud *et al.* (1993) and Bolze *et al.* (2001). The measured XR data were analyzed quantitatively with a recursive formula given by the dynamic theory of Parratt (1954), which properly incorporates absorption, refraction and multiple scattering effects. Interfacial roughness was taken into account by introducing Névot–Croce damping factors into the recursive formula, assuming Gaussian smearing functions (Névot & Croce, 1980). In addition, TEM measurements were carried out using a JEM microscope (model 4000Fx) on samples prepared on carbon grids of 400 mesh by dip-coating in dilute solutions (1.0 wt% solid content). For some of the dried films, TGA measurements were performed at 2.0 K $min^{-1}$ in a nitrogen atmosphere using a Seiko TG/DT analyzer (Seiko Instruments, EXSTAR 6000 TG/DT).

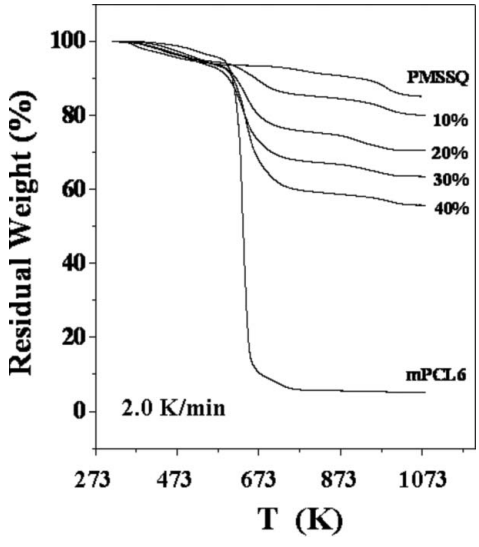


**Figure 2**
TGA thermograms of the PMSSQ precursor, mPCL6 porogen, and PMSSQ precursor/mPCL6 porogen blends. The measurements were carried out at a heating rate of 2 K $min^{-1}$ under a nitrogen atmosphere.

## 3. Results and discussion

Fig. 2 shows TGA thermograms of the PMSSQ precursor, mPCL6 porogen, and PMSSQ precursor/mPCL6 porogen blends. The mPCL6 porogen undergoes some weight loss in the temperature range 356–593 K owing to the evaporation of the ethanol by-product generated by the thermal curing reaction of the porogen's triethoxysilyl terminal groups, and exhibits significant weight loss above 593 K as a result of thermal decomposition. Similar weight loss behaviors were observed for mPCL6 porogen molecules loaded into a PMSSQ precursor matrix. The PMSSQ precursor also undergoes weight loss in the temperature range 348–613 K, which is attributed to the evaporation of the water and ethanol byproducts generated by the thermal curing reaction of the precursor's hydroxysilyl and ethoxysilyl end groups, and very slow thermal decomposition of the cured PMSSQ dielectric occurs above 773 K (Fig. 2). These TGA results indicate that during the heating run, both the mPCL6 porogen and the PMSSQ precursor components in the blend films undergo curing

reactions in the temperature range 356–593 K prior to the sacrificial thermal decomposition of the porogen component. This concurrence of the curing reactions of the porogen and precursor matrix components favors the chemical hybridization of the components, which prevents the formation of large porogen aggregates. On the basis of these TGA results, we prepared all of the porous PMSSQ dielectric films imprinted with mPCL6 porogen in a vacuum by thermal treatment up to 673 K.

Fig. 3 shows a TEM image of a porous PMSSQ sample imprinted with 10 wt% mPCL6 porogen, which is representative of the images recorded for the porous films. This TEM image clearly shows that closed, spherical pores with sizes of *ca* 5 nm were successfully generated in the dielectric film, and that these pores are randomly dispersed within the film.

Taking the above TGA and TEM results into account, specular XR measurements were carried out on the nanoporous PMSSQ dielectric films imprinted with various mPCL6 porogen loadings in order to obtain information on the structural parameters and interfaces of the films. Fig. 4(*a*) shows a representative XR profile curve, which was measured for a nanoporous PMSSQ film imprinted with an mPCL6 loading of 10 wt%. The figure clearly reveals two critical angles of the film and the substrate ($\theta_{c,film}$ and $\theta_{c,Si}$) over the $q_z$ range of 0.20−0.35 nm$^{-1}$; here $q_z$ is the magnitude of the scattering vector along the direction of the film thickness, which is defined by $q_z = (4\pi/\lambda)\sin(\theta)$, where $\lambda$ is the wavelength of the X-ray beam and $\theta$ is the grazing incident angle. Oscillations between the two critical angles are also clearly discernible, which are the waveguide modes for X-rays confined in the film. Thus, the reflected intensity is close to the incident one, although slightly lower owing to a certain degree of absorption of X-rays in the film. Once $\theta$ exceeds the critical angle of the substrate, a significant portion of the beam penetrates into the substrate and the reflected intensity drops sharply. The steeply decaying reflectivity curve is modulated by high frequency oscillations, which are commonly referred to as Kiessig fringes (Kiessig, 1931). These fringes appear owing to interference between the beams reflected from the film–air surface and those reflected from the film–substrate interface. It can be shown that, for a film of thickness $d$, the angular maximum position $\theta_{m,max}$ of the Kiessig fringe of order $m$ is given by $\sin^2(\theta_{m,max}) = m^2(\lambda/2d)^2 + \sin^2(\theta_{c,film})$. Thus, by plotting the experimental data according to this equation, the total film thickness can be precisely determined from the slope of a straight line fit of the data points. Using this approach, the total film thickness was very accurately determined to be 88.7±0.1 nm. In addition to the high frequency oscillations, low frequency oscillations are also discernible in Fig. 4(*a*), indicating that a thin layer (*i.e.* an interfacial layer) is present in addition to the film bulk layer. Further, it is noteworthy that as the angle increases, the XR profile shows an overall decay of the reflected intensity and of the modulation amplitudes, which can be attributed to the presence of the film–substrate interface and the surface roughness.

Considering the XR curve characteristics described above, we sought to quantitatively analyze the XR profile in Fig. 4(*a*). We found that the XR data are described well by the structural model shown in

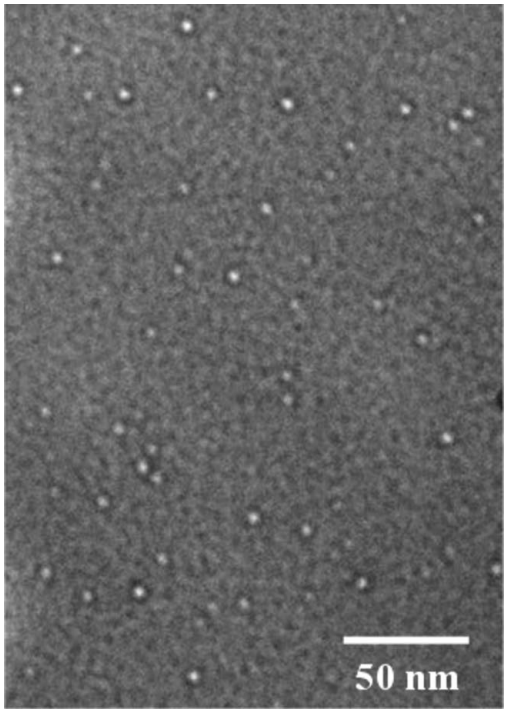


**Figure 3**
TEM image of a nanoporous PMSSQ dielectric prepared from a PMSSQ precursor sample loaded with 10.0 wt% mPCL6 porogen.

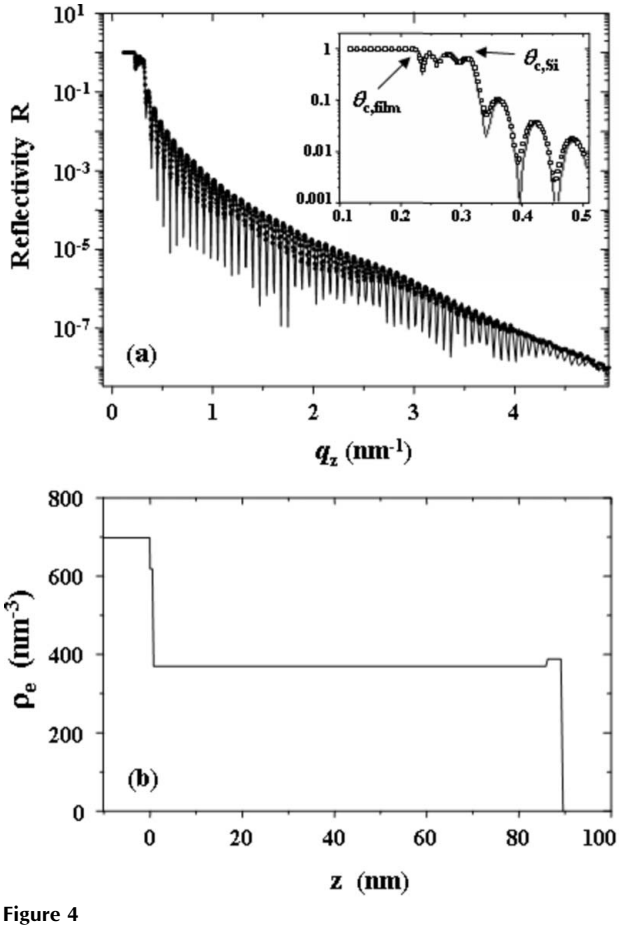


**Figure 4**
(*a*) A representative X-ray reflectivity profile of a nanoporous PMSSQ film imprinted with 10 wt% mPCL6. The symbols are the measured data and the solid line represents the fit curve assuming a homogeneous electron density distribution within the film except for a thin surface layer, in which the electron density is slightly different. The inset shows a magnification of the region around the two critical angles: $\theta_{c,film}$ is the critical angle of the film and $\theta_{c,Si}$ is the critical angle of the Si substrate. (*b*) A model of the electron density distribution across the film thickness between the silicon substrate and air, which gives the best fit for the XR profile in (*a*).

**Table 1**
Structural parameters and porosities of the PMSSQ film and the porous films imprinted with various mPCL6 porogen loadings, which were obtained by XR measurements and data analysis.

| mPCL6 loading (wt%) | $d$† (bulk) (nm) | $d$† (skin) (nm) | $\sigma$ ‡ (nm) | $\rho_e$(bulk)§ ($nm^{-3}$) | $\rho_e$(skin)§ ($nm^{-3}$) | $\rho_{e,av}$(film)§ ($nm^{-3}$) | $P_{rel}$¶ (vol%) |
|---|---|---|---|---|---|---|---|
| 0 | 81.1 | 4.9 | 0.4 | 396 | 443 | 399 | – |
| 10 | 85.4 | 3.3 | 0.6 | 369 | 388 | 370 | 7.3 |
| 20 | 82.0 | 7.0 | 1.8 | 316 | 268 | 312 | 21.8 |
| 30 | 90.5 | – | 2.9 | 264 | – | 264 | 33.8 |

† Thicknesses of bulk and skin layers. The uncertainty for the total film thickness is ±0.1 nm. ‡ Film surface roughness. § Electron densities of the bulk and the skin layer, and averaged over the entire film. The uncertainty for $\rho_{e,av}$ is ±5 $nm^{-3}$. ¶ Por-Porosity estimated with respect to the electron density of the PMSSQ film.

Fig. 4(*b*), which assumes a homogeneous electron density distribution throughout the film except for a thin surface skin layer characterized by a thickness of 3.3 nm and an electron density that is *ca* 5.1% higher than that of the bulk layer. The presence of this skin layer results in the low frequency modulation that was found to affect the whole XR curve, and the phase of this modulation unambiguously indicates that the electron density of the skin layer is slightly higher than that of the underlying bulk layer. The film surface roughness as determined from the decay of the XR curve is only 0.6 nm, indicating that the surface is very smooth. The fit curve based on the structural model [Fig. 4(*b*)] matches the experimental data very well, indicating that the model takes into account the key features of the system, including the surface roughness. In fact, a disparity between the model and experiment, however, is the depth of the minima, which are considerably shallower in the experimental data. The shallower depth of the minima in the experimental XR data may be due to several factors, such as a slightly inhomogeneous film thickness on the length scale of the projected beam size, curvature of the film-covered substrate induced by residual stress built up at the interface, and so on; however, a detailed investigation of this issue would be required to resolve the exact source of the shallower minima. Collectively, the XR data and analysis results indicate that a well-defined structure was developed in the porous film imprinted with 10 wt% mPCL6 porogen. The details of the structural parameters obtained are given in Table 1.

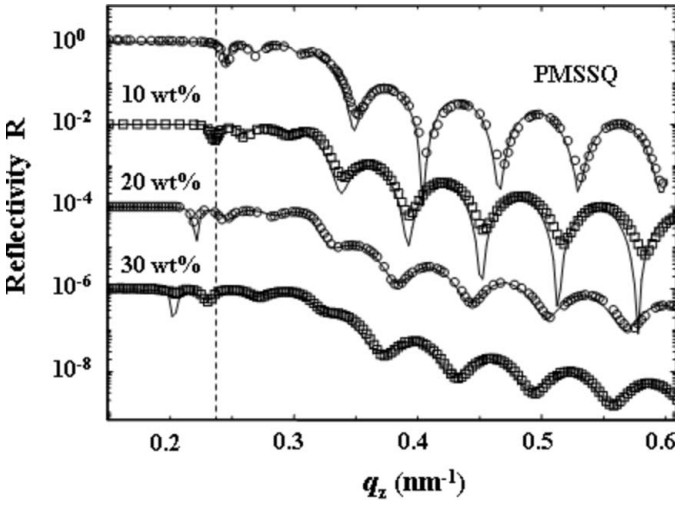


**Figure 5**
XR data around the two critical angles obtained from the films prepared with initial porogen loadings of 0 (PMSSQ), 10, 20 and 30 wt%. The symbols are the measured data and the solid lines represent the respective fit curves.

Here it is noteworthy that the presence of a thin surface skin layer with a slightly higher electron density in the above XR analysis is only one possible interpretation of the experimental data. Alternatively, the XR data can also be fitted by a model having a thin layer between the bulk of the film and the substrate, with a lower electron density (*ca* 5.1% is lower than that of the bulk layer). Furthermore, a model which incorporates both, such an interlayer and an additional surface skin layer, can fit the XR curve. This remaining ambiguity is due to the loss of phase information, and thus an electron density profile deduced from XR data is usually not unique (Bolze *et al.*, 2001). Once a location of such thin interfacial layer is given, the phase of the corresponding oscillation unambiguously indicates whether the electron density of that layer is higher or lower as compared with the bulk of the film. However, a skin-layer formation is often observed in the preparation of polymer specimens or products in any shapes including thin films (Clark & Feast, 1978; Fleer *et al.*, 1993). The presence of a thin interfacial layer was also detected even in the PMSSQ film of our study, which was prepared without any porogen loading. Moreover, at this moment we could not find any reason for the existence of a thin layer with a lower electron density at the interface of the substrate and the film layer. Considering this, we infer that the low frequency modulation of the reflectivity curve is originated from the presence of a thin skin layer.

For the PMSSQ film and the porous films imprinted with porogen loadings of 20 and 30 wt%, the whole XR profiles were analyzed in detail following the method outlined above for the porous film prepared using a porogen loading of 10 wt%. All of the films showed qualitatively similar characteristics in the whole XR profile (data not shown), as shown by the data displayed in Fig. 4(*a*). The detailed analysis results are listed in Table 1.

Fig. 5 shows the XR profiles around the critical angles of the films prepared with various porogen loadings, along with the fitted curves. All of the fits accurately capture the locations of the maxima and minima in the experimental data and allow precise determination of the respective film critical angles $\theta_{c,film}$ [*i.e.* average film electron densities $\rho_{e,av}$(film)]: $\theta_{c,film} = \lambda\sqrt{\rho_{e,av}(film) r_e/\pi}$ where $r_e$ is the classical electron radius. As the initial porogen loading increases, the film critical angle $\alpha_{c,film}$ clearly decreases, indicative of a decrease in the average film electron density, whereas the silicon substrate critical angle $\alpha_{c,Si}$ is insensitive to the initial porogen loading. The decrease in film electron density with increasing porogen content confirms that the porogen was removed by heat treatment up to 673 K and that pores were indeed created. The $\rho_{e,av}$(film) of the PMSSQ film prepared without any initial porogen loading was determined to be $399 \pm 5$ $nm^{-3}$ from the measured $\theta_{c,film}$. Using this value, one can further estimate the volume of the pores (*i.e.* porosity) imprinted in the porous films from the determined electron densities; here the estimated porosity corresponds to the relative porosity ($P_{rel}$) with respect to the electron density of the PMSSQ dielectric thin film. The estimated $P_{rel}$ values increase from 7.3% to 33.8% as the initial porogen loading is increased from 10 to 30 wt%, again confirming that the porogen molecules loaded in the PMSSQ films were effectively removed *via* sacrificial thermal degradation, leaving in their place nanopores filled with air that have almost zero electron density. All of the fit parameters and the estimated porosities are summarized in Table 1.

As can be seen in Table 1, the porogen-free PMSSQ film consists of a bulk layer covered with a skin layer of larger electron density, as was observed for the porous film imprinted with a 10 wt% porogen loading. The formation of such a denser skin layer on the PMSSQ film

might be due to the crosslinking reaction characteristic of the PMSSQ precursor occurring more favorably at the PMSSQ–air interface than in the bulk film as well as in the PMSSQ–substrate interface. However, the data in Table 1 show that both the skin and bulk layers in the film are significantly influenced during porous film formation by thermal sacrificial degradation of the porogen molecules loaded in the film. Namely, the thicknesses and electron densities of the skin and bulk layers are drastically changed with the initial porogen loading in the film formation process. In particular, the electron density of the skin layer [$\rho_e$(skin)], as well as the electron density of the bulk layer [$\rho_e$(bulk)], is decreased as the initial porogen loading increases. The skin layer of the PMSSQ film is thicker and its $\rho_e$(skin) value is larger, compared to the film imprinted with 10 wt% porogen. The porous film prepared with a porogen loading of 20 wt% also has a skin layer in addition to the bulk layer. This skin layer is thicker than the skin layers observed on the PMSSQ film and the porous film imprinted with 10 wt% porogen. Unlike the PMSSQ film and the porous film imprinted with 10 wt% porogen, however, the skin layer of the 20 wt% porogen film exhibits an electron density that is lower than that of the bulk layer. By contrast to the other films, the porous film imprinted with a 30 wt% porogen loading was found to have no skin layer. This observation of no skin layer might be attributed to the following situation. In the porous film process, a surface skin layer is formed, and its $\rho_e$(skin) is reduced by thermal sacrificial degradation of the loaded porogen molecules, finally reaching to a certain level, which is comparable to the $\rho_e$(bulk) value. Collectively, the characteristics of the skin layer in the PMSSQ film and its porous films are significantly influenced during porous film formation by out-gases generated from the thermal sacrificial degradation of the porogen molecules loaded in the film.

In addition, the surface roughnesses of the films increased with increasing porogen loading, from 0.4 nm for the PMSSQ film to 2.9 nm for the film with a porogen loading of 30 wt% (Table 1).

## 4. Conclusions

PMSSQ dielectric thin films with and without closed nanopores were prepared by the formation of blend films of thermally curable PMSSQ precursor and reactive mPCL6 porogen in various compositions, which were subsequently subjected to thermal treatment up to 673 K in a vacuum. The nanometer-scale structures of these thin films were investigated in detail by quantitative, non-destructive XR analysis along with TEM and TGA. The results indicated that thermal processing by heating to 673 K caused efficient sacrificial thermal degradation of the porogen molecules, generating closed, spherical nanopores in the dielectric film. The XR analysis showed that all of the nanoporous films exhibited a homogeneous, well-defined structure with a low surface roughness. The films imprinted with porogen loadings of 0–20 wt% were covered in a thin skin layer, but the film imprinted with a 30 wt% porogen loading did not have a skin layer. The film porosities ranged from 0 to 33.8% as the initial porogen loading was increased from 0 to 30 wt%.

This study was supported by the Ministry of Commerce, Industry and Resources (MCIR) and the Ministry of Science and Technology (MOST) (System IC 2010 Project), by the Korea Science and Engineering Foundation (National Research Lab Program and Center for Integrated Molecular Systems), and by the Korean Ministry of Education (Brain Korea 21 Program). The XR measurements were carried out at the Pohang Accelerator Laboratory (PAL) and the Stanford Synchrotron Radiation Laboratory, a national user facility operated by Stanford University on behalf of the US Department of Energy, Office of Basic Energy Sciences. The measurements at the PAL were supported by MOST and POSCO.

## References

Bolze, J., Kim, J., Huang, J.-Y., Rah, S., Youn, H. S., Lee, B., Shin, T. J. & Ree, M. (2002). *Macromol. Res.* **10**, 2–12.
Bolze, J., Ree, M., Yoon, H. S., Chu, S.-H. & Char, K. (2001). *Langmuir*, **17**, 6683–6691.
Clark, D. T. & Feast W. J. (1978). *Polymer Surfaces*. New York: Wiley.
Fleer, G. J., Cohen Stuart, M. A., Scheutjens, J. M. H. M., Cosgrove, T. & Vincent, B. (1993). *Polymers at Interfaces*. New York: Chapman and Hall.
Gibaud, A., Vignaud, G. & Sinha, S. K. (1993). *Acta Cryst.* A**49**, 642–648.
Harmer, M. A., Farneth, W. E. & Sun, Q. (1996). *J. Am. Chem. Soc.* **118**, 7708–7715.
Huang, E., Toney, M. F., Volksen, W., Mecerreyes, D., Brock, P., Kim, H.-C., Hawker, C. J., Hedrick, J. L., Lee, V. Y., Magbitang, T. & Miller, R. D. (2002). *Appl. Phys. Lett.* **81**, 2232–2234.
Hwang, Y., Heo, K., Chang, C. H., Joo, M. K. & Ree, M. (2006). *Thin Solid Films*, **510**, 159–163.
Kiessig, H. (1931). *Ann. Phys.* **10**, 769–788.
Lee, H.-J., Lin, E. K., Wang, H., Wu, W.-L., Chen, W. & Moyer, E. C. (2002). *Chem. Mater.* **14**, 1845–1852.
Lee, B., Oh, W., Hwang, Y., Park, Y.-H., Yoon, J., Jin, K. S., Heo, K., Kim, J., Kim, K.-W. & Ree, M. (2005). *Adv. Mater.* **17**, 696–701.
Lee, B., Oh, W., Yoon, J., Hwang, Y., Kim, J., Landes, B. G., Quintana, J. P. & Ree, M. (2005). *Macromolecules*, **38**, 8991–8995.
Lee, B., Park, Y.-H., Hwang, Y.-T., Oh, W., Yoon, J. & Ree, M. (2005). *Nat. Mater.* **4**, 147–150.
Lee, B., Shin, T. J., Lee, S. W., Yoon, J., Kim, J. & Ree, M. (2004). *Macromolecules*, **37**, 4174–4184.
Lee, B., Yoon, J., Oh, W., Hwang, Y., Heo, K., Jin, K. S., Kim, J., Kim, K.-W. & Ree, M. (2005). *Macromolecules*, **38**, 3395–3405.
Lev, O., Tsionsky, M., Rabinovich, L., Glezer, V., Sampath, S., Pankratov, I. & Gun, J. (1995). *Anal. Chem.* **67**, 22–30.
Morais, T. D. de, Chaput, F., Bailot, J.-P., Lahlil, K., Darracq, B. & Levy, Y. (1999). *Adv. Mater.* **11**, 107–112.
Névot, L. & Croce, P. (1980). *Rev. Phys. Appl.* **15**, 761–769.
Oh, W., Hwang, Y.-T., Park, Y. H., Ree, M., Chu, S.-H., Char, K., Lee, J.-K. & Kim, S. Y. (2003). *Polymer*, **44**, 2519–2527.
Parratt, L. G. (1954). *Phys. Rev.* **95**, 359–369.
Ree, M. & Ko, I. S. (2005). *Phys. High Tech. (Korea)*, **14**, 2–7.
Ree, M., Yoon, J. & Heo, K. (2006). *J. Mater. Chem.* **16**, 685–697.
Rottman, C., Grader, G., DeHazan, Y., Melchior, S. & Avnir, D. (1999). *J. Am. Chem. Soc.* **121**, 8533–8543.
Shin, Y. C., Choi, K.-Y., Jin, M. Y., Hong, S.-K., Cho, D., Chang, T. & Ree, M. (2001). *Korea Polym. J.* **9**, 100–106.
Smaihi, M., Jermoumi, T., Marignan, J. & Noble, R. D. (1996). *J. Membr. Sci.* **116**, 211–220.